Proceedings of the ASME 2017 36th International Conference on Ocean, Offshore and Arctic Engineering
OMAE2017
June 25-30, 2017, Trondheim, Norway

OMAE2017-61725

TIME-DOMAIN ANALYSIS OF WIND-INDUCED RESPONSE OF A SUSPENSION BRIDGE IN COMPARISON WITH THE FULL-SCALE MEASUREMENTS

Jungao Wang
Department of Mechanical and
Structural Engineering and Materials Science
University of Stavanger
NO-4036, Stavanger, Norway

Etienne Cheynet
Department of Mechanical and
Structural Engineering and Materials Science
University of Stavanger
NO-4036, Stavanger, Norway

Jasna Bogunović Jakobsen
Department of Mechanical and
Structural Engineering and Materials Science
University of Stavanger
NO-4036, Stavanger, Norway

Jónas Snæbjörnsson[1,2]
[1]School of Science and Engineering
Reykjavík University
IS-101 Reykjavík, Iceland
[2]Department of Mechanical and
Structural Engineering and Materials Science
University of Stavanger
NO-4036, Stavanger, Norway

ABSTRACT

The present study compares the buffeting response of a suspension bridge computed in the time-domain with full-scale measurement data. The in-service Lysefjord Bridge is used as a study case, which allows a unique comparison of the computational results with full-scale buffeting bridge response observed during a one year monitoring period. The time-domain analysis is performed using a finite element approach. Turbulent wind field is simulated according to the governing bridge design standard in Norway for three different terrain categories. The time-domain analysis indicates that the non-linear components of the wind loading are of limited importance in the present case, contributing by less than 5% to the standard deviation of the lateral displacement. The contribution of the buffeting loads on the main cables, hangers and towers to the lateral dynamic response of the bridge girder is about 6%. With the time-domain method, mode coupling as well as the influence of cables and towers are well captured in the simulation results. The buffeting response, estimated in terms of the standard deviation of acceleration, is found to be in good agreement with the field measurement data. Comparison suggests that the proposed numerical method, with the non-linear force model, is able to predict the bridge response reasonably well.

Keywords: suspension bridge, time domain, finite element model, buffeting response, field measurement

INTRODUCTION

The Norwegian Public Road Administration is considering building long-span floating suspension bridges in Western Norway to cross deep fjords that are up to around 5 km wide. Such bridges will have eigen-frequencies as low as 0.01 Hz. They are therefore extremely wind sensitive structures which require a dedicated investigation of wind-induced effects.

The buffeting theory, introduced more than 50 years ago by

Davenport [1] and further developed by e.g. Scanlan [2] is a standard approach to evaluate the bridge dynamic response due to wind turbulence. The buffeting bridge response is among the governing design factors in the ultimate limit state.

There have been growing researches on the numerical methods accounting for bridge buffeting response in the last few decades. The frequency domain method has been applied since the 80's and is an effective tool using the linear buffeting force model [3–5]. More recent developments based on the time-domain approach have been carried out by e.g. [6–9]. Comparisons between full-scale measurements and computed bridge response are seen in [5, 10, 11], however, mostly limited to only a few hour to a few days of data. To the authors' knowledge, there is no such comparison for data set made of long period full-scale bridge measurements.

Since 2013, the research group from University of Stavanger has started the field measurement campaign on both wind field characteristics and bridge response at the Lysefjord Bridge, which is located at a narrow inlet of a fjord in the South-West of the Norwegian coast [10]. The present paper compares thousands of full-scale acceleration records obtained during the year 2015 on the Lysefjord Bridge with time-domain numerical predictions, aiming at validating the buffeting theory using long period full-scale data.

A numerical model based on the finite element method (FEM) is built to evaluate the wind-induced buffeting response of the bridge. The wind buffeting forces applied in the model are based on the quasi-steady theory. A turbulent wind field is simulated based on the turbulence spectra provided in the governing bridge design standard in Norway, i.e. Handbook N400 [12]. The calculations are performed for three different terrain categories, in order to explore which terrain category is most consistent with the observed bridge response. The influence of the wind buffeting force linearization as well as the contribution of the buffeting load from the girder, main cables, hangers and towers on the bridge girder response is discussed and summarized. Most importantly, the availability of the field measurement data allows us to assess the ability of the present finite element model (FEM) to estimate the bridge buffeting response.

1 THE BRIDGE PROPERTIES AND THE NUMERICAL MODEL

1.1 Lysefjord Bridge properties

The Lysefjord Bridge is built in a mountainous area in Norway, with a main span of 446 meters (Fig. 1). The bridge deck support at the north tower cross-beam is at a higher elevation (52.36 m) compared to that at the south tower (44.90 m). The deck mid-span is 53.37 m above the sea surface. The bridge girder is suspended from the two main cables by 35 hangers at each side. The main cables have a sag of 45 m with its lowest point 3 m above the bridge deck at mid-span, indicated by H-18 in Fig. 1.

TABLE 1. Physical properties of the Lysefjord Bridge girder and towers.

Item	Value
Girder	
Length (m)	446
Width (m)	12.3
Height (m)	2.76
Section weight (kg/m)	5350
Section area (m^2)	0.343
Vertical area moment of inertia (m^4)	0.429
Lateral area moment of inertia (m^4)	4.952
Torsional moment of inertia (m^4)	0.929
Section mass moment of inertia w/o cables (kgm)	4.952
Young's modulus (Nm^{-2})	2.1E11
Torsional modulus (Nm^{-2})	8.07E10
Towers	
Height (m)	102.26
Young's modulus (Nm^{-2})	4E10

The Lysefjord Bridge girder is made as a closed steel box with plate stiffeners and diaphragms at each 12 m. In this paper, the girder cross section has been simplified as a generalized beam with properties listed in Table 1 and Table 2. The two legs of each tower are connected by cross beams at the deck level and the top. They are made of concrete, with a cross-section area gradually decreasing with the increasing elevation. More details of the Lysefjord Bridge design, provided by Norwegian Public Road Administration, are included in e.g [13, 14].

1.2 Finite element model

Based on the above-mentioned bridge properties, a finite element (FE) model has been built in Abaqus [15] as shown in Figure 2. Beam elements (B31) are used to model the bridge girder, cables and towers with generalized cross section properties. The girder and each main cable consist of 39 nodes, and the girder has a characteristic element length of 12 m (only two elements at each end have a length of 7 m). Dummy mass elements are used to achieve the correct polar mass moment inertia of the girder and to provide the lower connection points for the hangers. The boundary conditions at tower bases and back-stay cable anchors consist of all six degrees of freedom being fixed. Both ends of the girder are coupled with the towers in a way that allows one end to

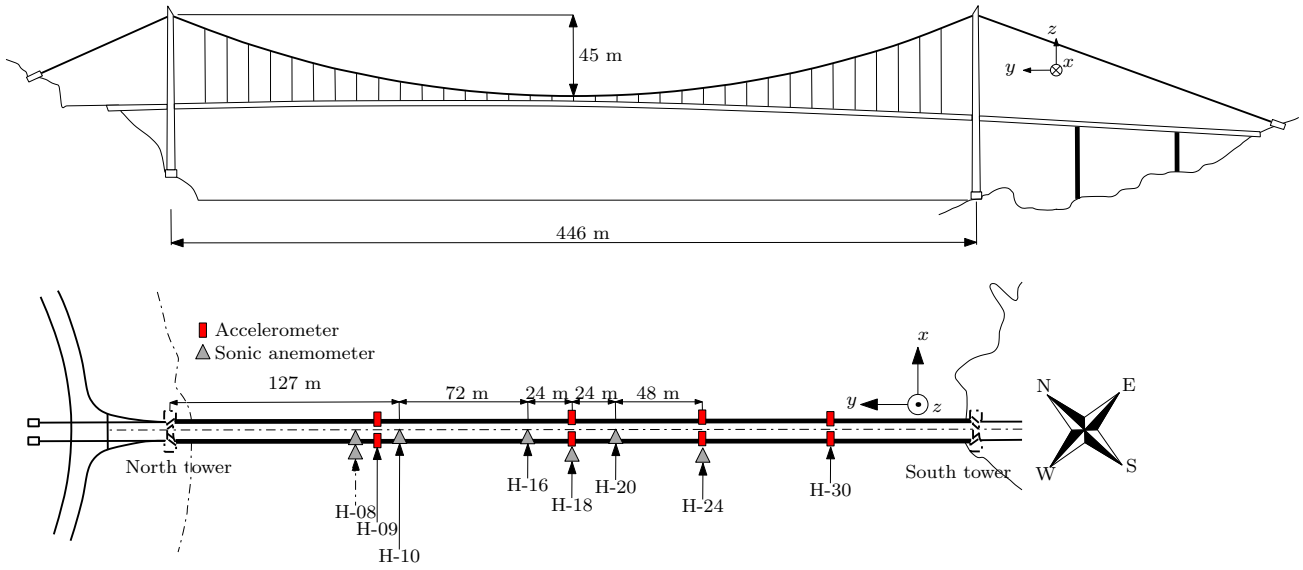

FIGURE 1. Elevation and plane-view of the Lysefjord Bridge.

move in the longitudinal direction.

It is important to achieve the correct static state of a suspension bridge before modal and dynamic analysis, as well as the non-linear properties of the hangers, which can only sustain tension forces. These characteristics have been considered in the numerical modelling of the bridge. Table 3 summarizes several of the lowest eigen-frequencies of the Lysefjord Bridge obtained using the FE-based software Alvsat and Abaqus. It shows that the implementation of flexible towers affects the general dynamic behavior of the bridge. The Abaqus model with flexible towers has the best overall agreement with the eigen-frequencies identified from field measurements [10]. Such a model also provides a more complete set of eigen-frequencies compared to frequently used models with rigid towers [13]. Therefore, the full bridge model build in this paper is not only useful for the time-domain analysis, but can also provide more accurate modal properties for frequency-domain analysis.

The Rayleigh damping model is used to account for the structural damping of the bridge, which was targeted at 0.5% damping ratio.

2 WIND FIELD CHARACTERISTICS AND THE BUFFETING THEORY

2.1 Wind field description

According to [16], wind measurements at Lysefjord Bridge indicate that the wind field in the fjord is strongly affected by the complex terrain characteristics, such as the alignment of the fjord, steep mountain valleys and the proximity of an island in the narrow fjord. Consequently, the measured flow at the bridge site is rather turbulent, in particular in the case of wind from North-East direction. In this paper, the applicability of the empirical wind model recommended by the Norwegian Public Road Administration Handbook N400 [12] is assessed by comparing the computed bridge response with the measured one. According to N400, the normalized wind spectrum for $i = \{u, v, w\}$ (where u, v, w denotes the along-wind, across-wind and vertical wind components) is expressed as

$$\frac{fS_i(f)}{\sigma_i^2} = \frac{A_i f_i}{(1+1.5A_i f_i)^{5/3}} \tag{1}$$

where S_i is the Power Spectral Density (PSD) of the turbulent wind component at different frequencies; σ_i is the standard deviation of the wind turbulence; A_i is the empirical parameter representing the different wind component with $A_u = 6.8$, $A_v = 9.4$ and $A_w = 9.4$; f_i is the non-dimensional frequency which can be expressed as

$$f_i = \frac{fL_i^x(z)}{\overline{u}(z)} \tag{2}$$

where L_i^x is the height-dependent turbulence length scale in the along-wind direction, which represents the "average gust size" for natural wind; $\overline{u}$ is the height-dependent mean wind velocity. The mean wind velocity $\overline{u}(z)$ is calculated as

$$\overline{u}(z) = U_{ref}\kappa_T \ln(z/z_0) \tag{3}$$

where U_{ref} is the reference mean wind velocity (i.e. the 10 min mean wind velocity at the height of 10 m for terrain category

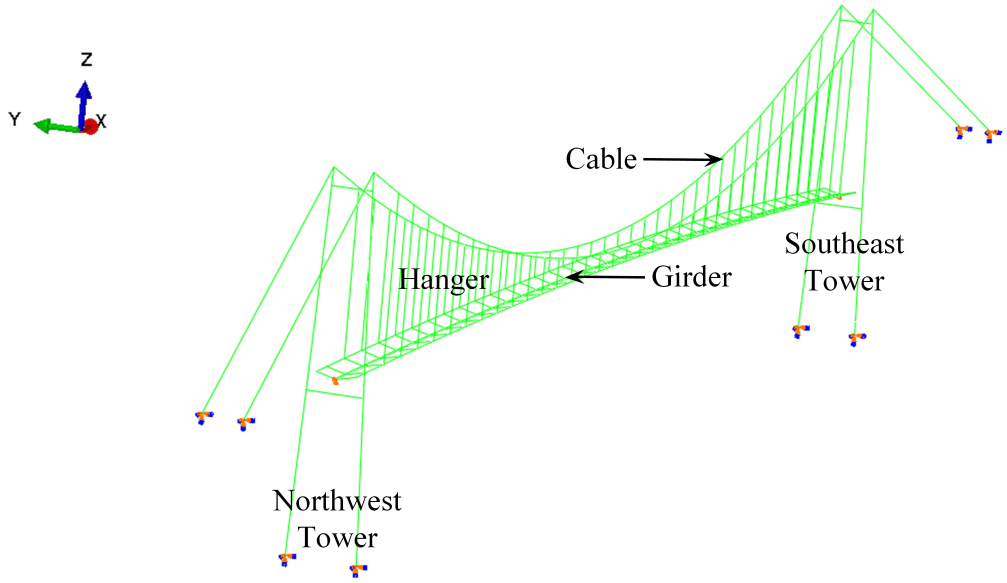

FIGURE 2. Lysefjord bridge model sketch in ABAQUS.

2, with the annual probability of exceedance of 0.02); κ_T is the terrain factor (the ratio of the surface roughness and the von Kármán constant) that depends on the terrain category; z_0 is the roughness length, which depends on the terrain category.

The length scales for different wind turbulence components in Eq. 2 can be expressed as

$$L_u^x = \begin{cases} L_1 \left(z/z_1\right)^{0.3}, & \text{if } z > z_{min}. \\ L_1 \left(z_{min}/z_1\right)^{0.3}, & \text{if } z \le z_{min}. \end{cases} \tag{4}$$

$$L_v^x = \frac{1}{4} L_u^x \tag{5}$$

$$L_w^x = \frac{1}{12} L_u^x \tag{6}$$

where L_1 is the reference length scale equal to 100 m; z_1 is the reference height equals to 10 m. z_{min} is an arbitrary minimal height that depends on the terrain category.

The turbulence intensity for different wind components is

$$I_u = \frac{\sigma_u}{\overline{u}} = \begin{cases} c_{tt} \ln\left(z/z_1\right), & \text{if } z > z_{min}. \\ c_{tt} \ln\left(z_{min}/z_1\right), & \text{if } z \le z_{min}. \end{cases} \tag{7}$$

$$I_v = \frac{3}{4} I_u \tag{8}$$

$$I_w = \frac{1}{2} I_u \tag{9}$$

where c_{tt} is the turbulence factor that depends on the terrain category [17].

Besides the single-point wind statistics described above, the correlation of wind gusts at different locations is also fundamental to access the wind load on the entire structure. According to N400, the co-coherence function of turbulence components at two points separated by distance is defined as

$$\gamma_i = \mathrm{Re}\left[\frac{\mathbf{S}_{i_1 i_2}(f, d_j)}{\sqrt{\mathbf{S}_{i_1}(f) \cdot \mathbf{S}_{i_2}(f)}}\right] \tag{10}$$

$$= \exp\left(-C_{ij} \frac{f d_j}{\overline{u}}\right) \tag{11}$$

where $i = \{u, v, w\}$, $j = \{y, z\}$; γ_i is the co-coherence,depending on the frequency f and the Euclidian distance d_j between the two points; $\mathbf{S}_{i_1}$ and $\mathbf{S}_{i_2}$ are the underlying single point power spectrum densities of the wind turbulence for the component i; $\mathbf{S}_{i_1 i_2}$ is the co-spectrum of turbulence at two different points. The co-coherence function decays with increasing distance and increasing frequency. The parameter C_{ij} is the decay coefficient, the values of which (for each wind component and wind direction) is provided by N400 and recalled in Table 4.

In this paper, we have selected three terrain categories (category 2, category 3 and category 4, denoted as N400C2, N400C3 and N400C4 respectively). It is of interest to know how the bridge response varies based on the choice of different terrain categories.

TABLE 2. Physical properties of the Lysefjord Bridge main cables, backstay cables and hangers.

Item	Value
Main cables	
Length (m)	459
Sag (m)	45
Section weight (kg/m)	816
Section area (m^2)	0.44
Bending moment of inertia (m^4)	2.6E-7
Young's modulus (Nm^{-2})	1.8E11
Torsional modulus (Nm^{-2})	8.07E10
Backstay cables	
Length (north cable) (m)	73.91
Length (South cable) (m)	166.05
Hangers	
Section weight (kg/m)	95
Section area (m^2)	0.0018
Bending moment of inertia (m^4)	2.6E-7
Young's modulus (Nm^{-2})	1.8E11
Torsional modulus (Nm^{-2})	8.07E10

TABLE 3. Measured and computed eigen-frequencies of the Lysefjord Bridge using different models.

	Alvsat with rigid towers (Hz)	Identified (Hz)	Abaqus with rigid towers (Hz)	Abaqus with flexible towers (Hz)
HS1	0.130	0.133	0.129	0.128
HA1	0.442	0.438	0.438	0.432
VA1	0.213	0.222	0.214	0.214
VS1	0.286	0.293	0.328	0.293
TS1	1.154	1.234	1.260	1.228
TA1	2.125	2.180	2.146	2.158

To estimate the bridge buffeting response in the time domain, a turbulent wind field is simulated for the whole structure, using the method proposed by [18, 19] based on the spectral model provided by N400. The wind field grid is overlapped with the bridge FEM nodes. The simulated wind field is assumed homogeneous, stationary and based on 10 min averaging time. It should be mentioned that there is a yaw angle between the mean wind direction and the girder normal direction based on the wind measurement at Lysefjord Bridge site. This angle is small and varying at different time windows. For all the numerical cases presented in this paper, the mean wind incident direction is assumed perpendicular to the bridge girder, therefore, wind loads caused by the cross-wind component (v component) are neglected. Finally, the cross-spectral density of wind turbulence is assumed negligible, as suggested by [20].

TABLE 4. Exponential decay coefficients given by N400 for the estimation of the wind coherence.

Coefficient	C_{uy}	C_{vy}	C_{wy}	C_{uz}	C_{vz}	C_{wz}
Value	10	6.5	6.5	10	6.5	3.0

Figure 3 presents the targeted N400C3 spectral functions (solid lines) and the simulated wind spectra (dashed lines, representing an average of four time histories) for comparison. Although the agreement between the two is good in the high frequency range, some discrepancies are noticeable at low frequencies (below 0.04 Hz for the along-wind direction and 0.05 Hz to 0.1 Hz for the vertical direction). The differences are partly due to the relatively coarse frequency resolution (0.0017 Hz) bound by the short duration (10 min) for the wind simulation and the number of cases considered (only four). These discrepancies are not likely to have a major influence on the Lysefjord Bridge buffeting response because of its relatively high eigen-frequencies. However, for future longer fjord-crossings with the lowest eigen-frequency of the order of 0.01 Hz, a longer simulation time window is suggested, to better describe the low frequency components of the simulated turbulent wind field.

Figure 4 presents the simulated wind characteristics, at different bridge element nodes, for terrain category 3 and $U_{ref} = 15$ m/s. As expected, the mean velocity increases and the turbulence intensity decreases with increasing height. At the bridge girder elevation, the turbulence intensities vary between 0.16 to 0.2 in the along-wind direction, and are around 0.09 for the vertical turbulence component.

2.2 Bridge buffeting force model with/ without linearization

It should be noted that the quasi-steady assumption is adopted and only the linear quasi-steady aerodynamic coefficients are used in the present study, as summarized in Table 5 [21].

Meanwhile, a damping term related to $k_0 Brx$ is introduced in the calculation of the buffeting overturning moment, where k_0 is

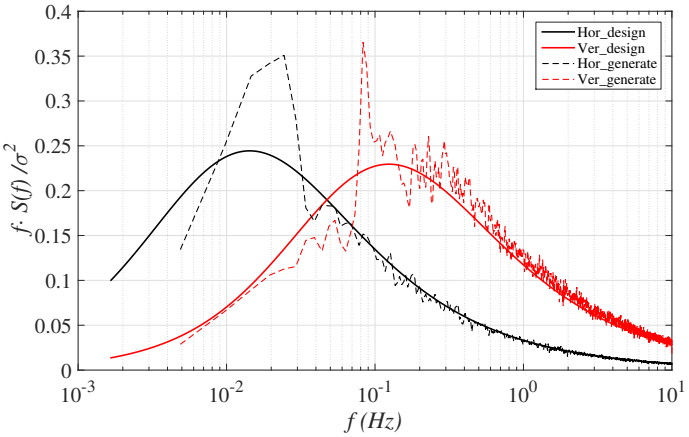

FIGURE 3. Comparison of the N400C3 wind spectrum and the spectrum based on the generated wind time histories at the mid-span of the bridge girder when $U_{ref} = 15$ m/s.

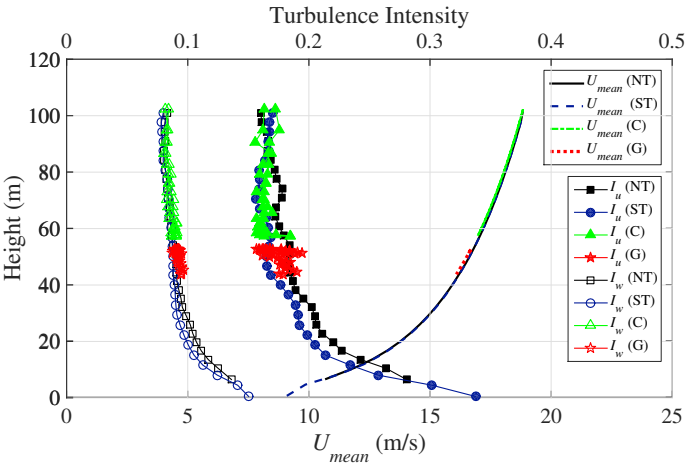

FIGURE 4. Wind characteristics (mean wind velocity, along-wind and vertical turbulence intensity) at different bridge locations (NT: north tower; ST: south tower; C: cable; G: girder) for N400C3, $U_{ref} = 15$ m/s.

TABLE 5. Quasi-steady aerodynamic coefficients for the Lysefjord Bridge.

Coefficient	C_D	C_L	C_M	$\frac{\partial C_D}{\partial \alpha}$	$\frac{\partial C_L}{\partial \alpha}$	$\frac{\partial C_M}{\partial \alpha}$
Girder	1.0	0.1	0.02	0	3	1.12
Cable	1.0	–	–	–	–	–
Hanger	1.0	–	–	–	–	–
Tower	1.2	–	–	–	–	–

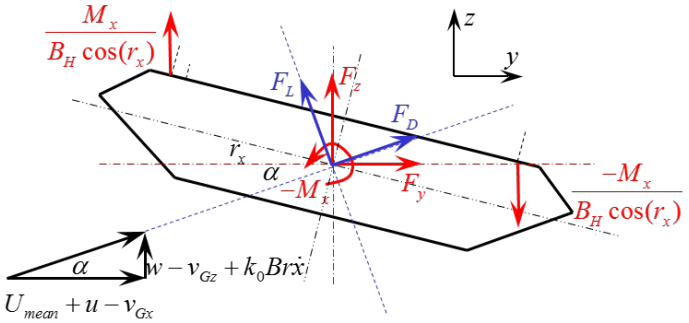

FIGURE 5. Force components of the bridge girder cross section subjected to wind load.

the horizontal distance between the aerodynamic and the shear center, which is set as 0.25 in the current study, B is the width of the girder and $r\dot{x}$ is the torsional velocity. Fig. 5 illustrates the wind force components on the girder cross-section.

In Fig. 5, the instantaneous wind-girder angle includes two parts: the torsional displacement rx , and the instantaneous angle α due to the wind turbulence. Fig. 5 uses the same right-hand coordinate as that in Abaqus, therefore, rx and $r\dot{x}$ are positive anti-clockwise. This has been considered when calculating the associated forces in Eq. 12. Therefore, the associated drag, lift and overturning moment at the girder shear center can be expressed as

$$\begin{bmatrix} F_D(t) \\ F_L(t) \\ M_x(t) \end{bmatrix} = \frac{1}{2}\rho U_{tot}^2(t) B \begin{bmatrix} \frac{H}{B} C_D(\alpha(t) - rx(t)) \\ C_L(\alpha(t) - rx(t)) \\ B C_M(\alpha(t) - rx(t)) \end{bmatrix} \tag{12}$$

where the three aerodynamic coefficient derivatives with respect to the angle of attack are denoted as C'_D, C'_L and C'_M. The instantaneous effective wind velocity $U_{tot}(t)$ can be calculated by

$$|U_{tot}|^2 = [\bar{u} + u(t) - \dot{y}(t)]^2 + [w(t) - \dot{z}(t) + k_0 B r\dot{x}(t)]^2 \tag{13}$$

These forces are then decomposed into horizontal and vertical components

$$\begin{bmatrix} F_y(t) \\ F_z(t) \end{bmatrix} = \begin{bmatrix} \cos(\alpha(t)) & -\sin(\alpha(t)) \\ \sin(\alpha(t)) & \cos(\alpha(t)) \end{bmatrix} \begin{bmatrix} F_D(t) \\ F_L(t) \end{bmatrix} \tag{14}$$

The overturning moment is applied by a pair of vertical forces at the hanger connection point, as shown in Figure 5, with the force magnitude calculated by

$$F_{Hy}(t) = \frac{M_x(t)}{B_H \cos(rx(t))} \tag{15}$$

Eqs. 12 to 15 are the full expressions of the applied wind buffeting forces in time-domain. It can be observed that all the three force components in Eq. 12 have time-dependent elements on the right hand of the equations, which are related to the girder motion terms, known as motion-dependent forces. In the time-domain buffeting analysis in Abaqus, these motion-dependent forces are calculated at each time step and applied to the elements using a user-defined subroutine. For the cable, hanger and tower elements, only the mean and the fluctuating drag forces are considered, using a similar approach as that for the girder.

In the expression for the total velocity U_{tot} in Eq. 13, there are non-linear terms of wind turbulence and girder motions, which have to be linearized when the frequency domain approach is used [10]. The linearized forces are given in Eqs. 16 to 20. Eq. 17 gives the static wind load, Eq. 18 represents the buffeting load, Eq. 19 shows the aerodynamic damping matrix and Eq. 20 stands for the aerodynamic stiffness.

$$\mathbf{F} = \mathbf{A_0}\left[\overline{u}\right] + \mathbf{A_1}\begin{bmatrix} u(t) \\ w(t) \end{bmatrix} - \mathbf{C_{ae}}\begin{bmatrix} \dot{y(t)} \\ \dot{z(t)} \\ \dot{rx(t)} \end{bmatrix} - \mathbf{K_{ae}}\begin{bmatrix} y(t) \\ z(t) \\ rx(t) \end{bmatrix} \tag{16}$$

where:

$$\mathbf{A_0} = \frac{1}{2}\rho\overline{u}B\begin{bmatrix} \frac{H}{B}C_D \\ C_L \\ BC_M \end{bmatrix} \tag{17}$$

$$\mathbf{A_1} = \frac{1}{2}\rho\overline{u}B\begin{bmatrix} 2\frac{H}{B}C_D & \left(\frac{H}{B}C'_D - C_L\right) \\ 2C_L & \left(C'_L + \frac{H}{B}C_D\right) \\ 2BC_M & BC'_M \end{bmatrix} \tag{18}$$

$$\mathbf{C}_{ae} = \frac{1}{2}\rho\overline{u}B\begin{bmatrix} 2\frac{H}{B}C_D & \frac{H}{B}C'_D - C_L & k_0B\left(\frac{H}{B}C'_D - C_L\right) \\ 2C_L & C'_L + \frac{H}{B}C_D & k_0B\left(C'_L + \frac{H}{B}C_D\right) \\ 2BC_M & BC'_M & k_0B^2C'_M \end{bmatrix} \tag{19}$$

$$\mathbf{K}_{ae} = -\frac{1}{2}\rho\overline{u}^2B\begin{bmatrix} 0 & 0 & \frac{H}{B}C'_D \\ 0 & 0 & C'_L \\ 0 & 0 & BC'_M \end{bmatrix} \tag{20}$$

3 RESULTS AND DISCUSSION

Time-domain methods considering both linear and nonlinear buffeting force model are applied to investigate the buffeting response of the Lysefjord Bridge to understand the effect of the non-linear terms of the wind buffeting loads. The influence of the wind loads from the main cables, hangers and towers on the bridge girder response is also studied. Furthermore, numerical results considering different mean wind velocities and terrain categories are compared with the field measurement data acquired over a period of one-year in 2015.

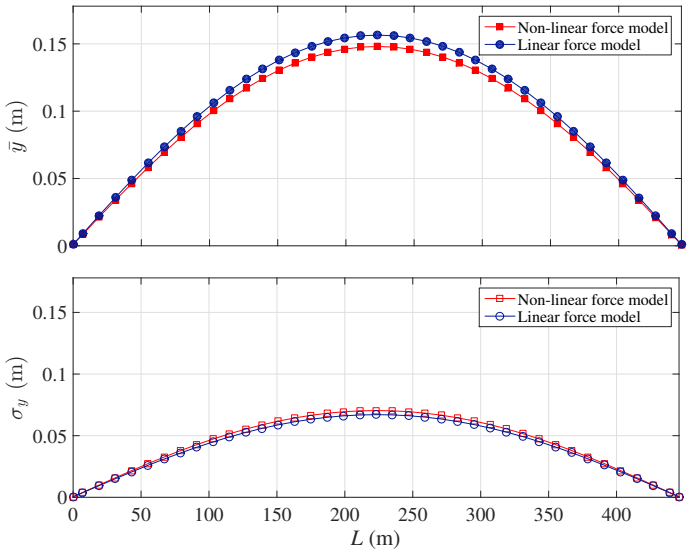

FIGURE 6. Wind induced lateral displacement of the bridge girder, evaluated using time domain simulation with linear and non-linear force models (top: mean lateral displacement comparison; bottom: lateral displacement standard deviation comparison).

3.1 Influence of the linearization of the wind buffeting forces

Fig. 6 presents the comparison of the girder lateral displacement estimated using linear and non-linear force models, whereas Fig. 7 presents the comparison of the PSDs of the girder lateral displacement at the mid-span. The results for the vertical and the torsional response are given in Figs. 8 to 11 respectively. The wind field simulated for a terrain category 3 with $U_{ref} = 15$ m/s has been used for this study on wind load linearization effect.

Comparison in Fig. 6 indicates that the mean lateral displacement using the non-linear force model is smaller than the one using linear force model, but the standard deviation (std) is slightly larger with the linear force model than without. Comparison of the PSDs in Fig. 7 shows a good agreement between the two methods at capturing the response at dominant eigenfrequency, corresponding to mode HS1 in Table 3. Frequency components associated with the higher symmetric modes HS2 and HS3 are also visible. Another response frequency component, corresponding to mode TS1 is also quite significant in the spectrum, due to a structural coupling, i.e. a minor horizontal

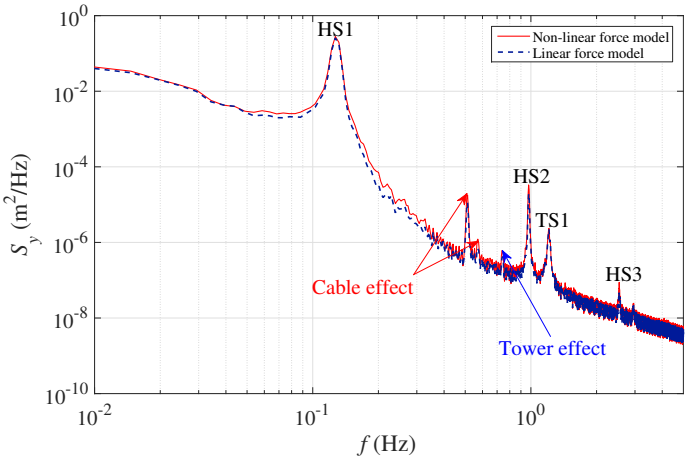

FIGURE 7. Power spectral density of the bridge girder lateral displacement, evaluated using time domain simulation with linear and non-linear force models.

component of the TS1 mode. There are also some spectral peaks capturing the cable or tower dominant lateral modes, involving some lateral motion of the girder, as marked in Fig. 7.

The comparison of the vertical response in Fig. 8 shows that different force models give rather consistent results, with almost invisible differences. The displacement estimated using a non-linear force model is slightly larger than that from the linear force model. The comparison of the vertical displacement PSDs in Fig. 9 substantiates the good agreement seen in Fig. 8. The first six of the vertical symmetric eigen-frequencies are captured, as marked in Fig. 9.

The comparison of the calculated torsional displacements in Fig. 10 again shows good agreement among the results obtained by different force models, where only minor discrepancies are observed. Good agreement is also observed in the PSDs in Fig. 11 for the torsional motion, which clearly shows a mode coupling with mode HS1. This is because the first symmetric lateral mode includes a torsional component due to the "arch" shaped girder. Coupling with mode VS1 is also observed in the torsional response spectrum, due to the aerodynamic load coupling, as expressed in Eqs. 19-20. Other small frequency peaks are also identified, which are related to tower motion-induced girder torsions.

To quantify the influence of the linearization of the wind buffeting forces on the bridge response, we have summarized the results at the bridge girder mid-span, see Table 6. The response parameters are normalized with reference to the values obtained using a non-linear force model. The linearization of the buffeting wind forces leads to an overestimation of the mean lateral and torsional response by 6% and 2.6% respectively, and the underestimation of the mean vertical response by 2.1%. The standard deviation of the lateral, vertical and torsional response is

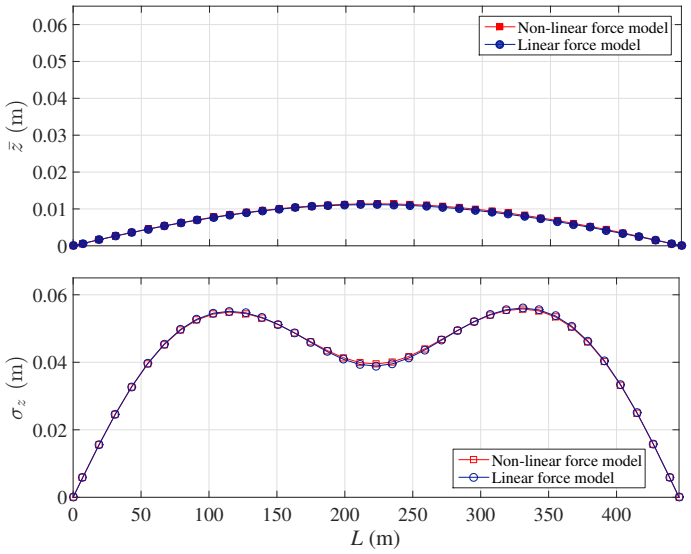

FIGURE 8. Wind induced vertical displacement of the bridge girder, evaluated using time domain simulation with linear and non-linear force models (top: mean vertical displacement; bottom: vertical displacement standard deviation).

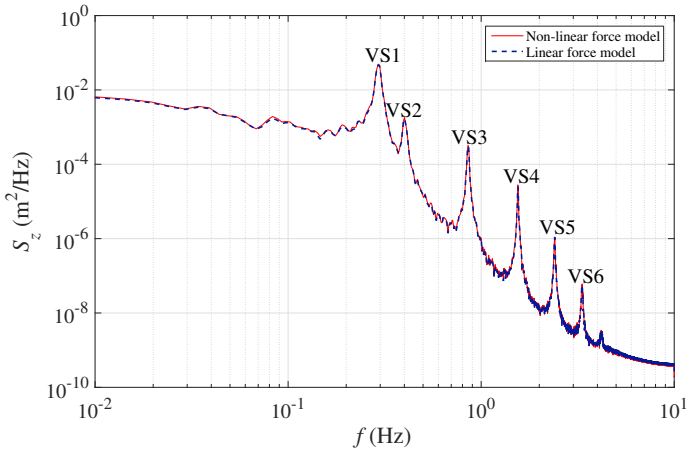

FIGURE 9. Power spectral density of the bridge girder vertical displacement, evaluated using time domain simulation with linear and non-linear force models.

TABLE 6. Difference of the bridge girder response at mid-span using the linear time domain approach compared to the non-linear force methods.

	$\bar{y}$	$\bar{z}$	$\overline{rx}$	σ_y	σ_z	σ_{rx}
Difference (%)	+6	-2.1	+2.6	-4.7	-1.5	-2.5

underestimated by 4.7%, 1.5% and 2.5% respectively.

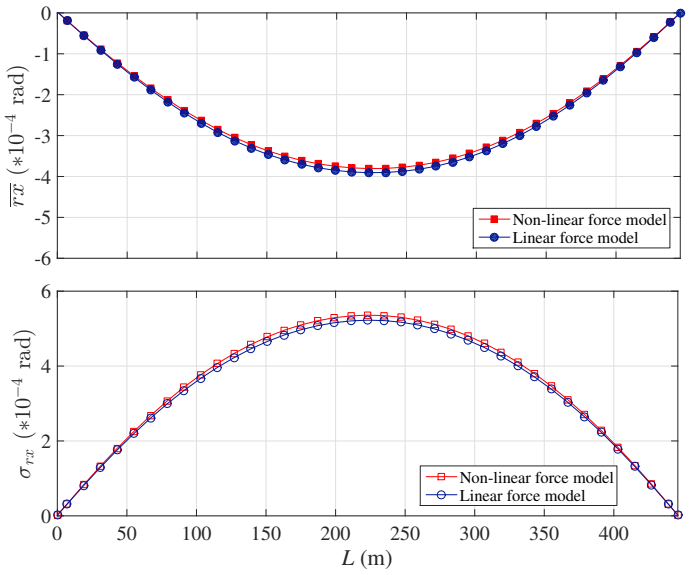

FIGURE 10. Wind induced torsional displacement of the bridge girder, evaluated using time domain simulation with linear and non-linear force models (top: mean torsional displacement; bottom: torsional displacement standard deviation).

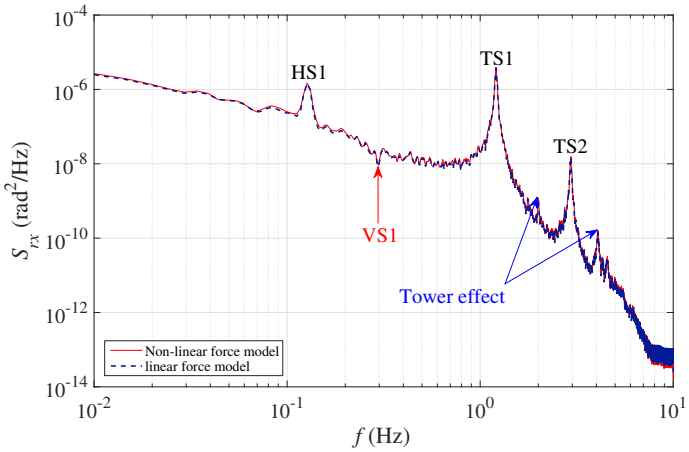

FIGURE 11. Power spectral density of the bridge girder torsional displacement, evaluated using time domain simulation with linear and non-linear force models.

3.2 Influence of wind loads from main cables, hangers and towers on the bridge girder response

The differences of the bridge girder response with and without wind loads on the cables, hangers and towers is investigated. All cases are based on the time-domain method using a non-linear force model considering the N400C3 wind parameters for $U_{ref} = 15$ m/s. The results for the lateral, vertical and torsional response are presented in Figs. 12 to 14 respectively. The cases

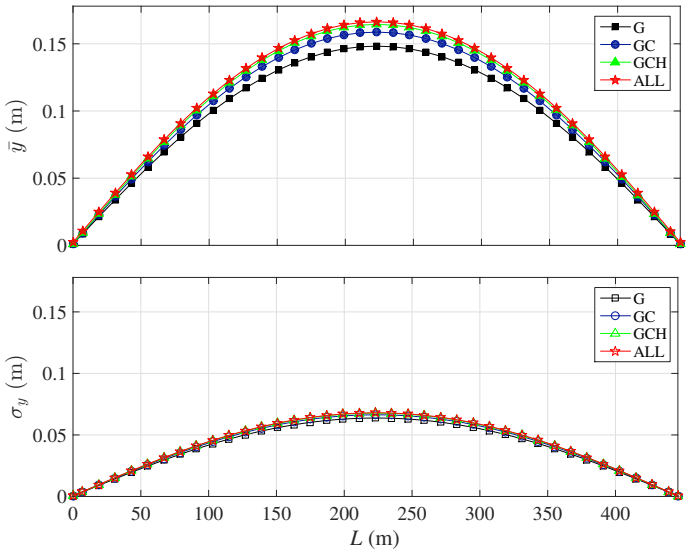

FIGURE 12. Wind induced lateral displacement of the bridge girder considering wind loads on the cable, hanger and tower (top: mean lateral displacement; bottom: lateral displacement standard deviation).

with wind loads on the girder only are denoted as "G" in the legend, "GC" stands for the girder and cable, "GCH" stands for the girder, cable and hanger and "ALL" stands for wind loads on the entire bridge.

Comparisons show that the wind loads on the main cables, hangers and towers mainly have an influence on the mean and fluctuating lateral response as well as the mean twisting response. This is partly because we assume the drag coefficient derivative and lift coefficient for the cable to be zero. A non-circular cross-section of the main cable would be exposed to increased vertical loads, and would therefore affect the vertical response of the girder to a greater extent.

Table 7 summarizes the bridge response at mid-span considering the wind loads on the main cables, hangers and towers. The response parameters are normalized with the values obtained considering the wind loads on the entire bridge structure. It can be observed that the mean and the fluctuating lateral, and the mean torsional response are primarily influenced by the wind loads on the main cables and hangers. The lateral and torsional mean values are underestimated by about 10% if only wind loads on the girder are considered. As for the dynamic lateral response, the wind loads from the main cables and hangers contribute to the entire response by 3.8% and 2% respectively. Their contribution to the dynamic vertical and torsional response is negligible, 0.3% and 0.2% respectively.

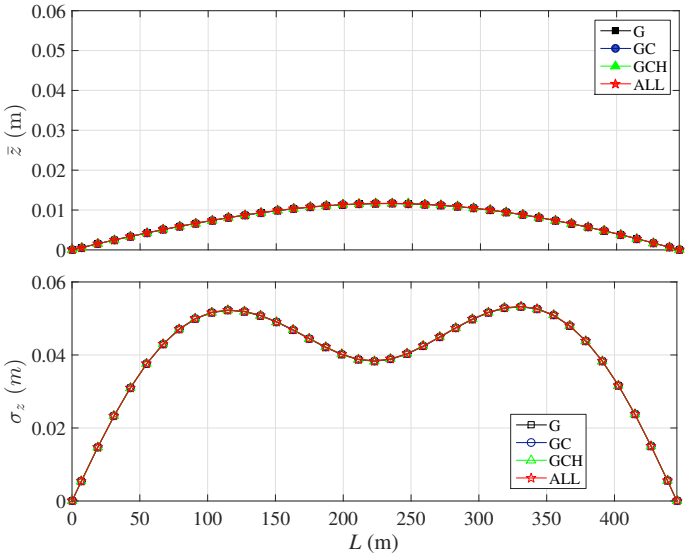

FIGURE 13. Wind induced vertical displacement of the bridge girder considering wind loads on the cable, hanger and tower (top: mean vertical displacement; bottom: vertical displacement standard deviation).

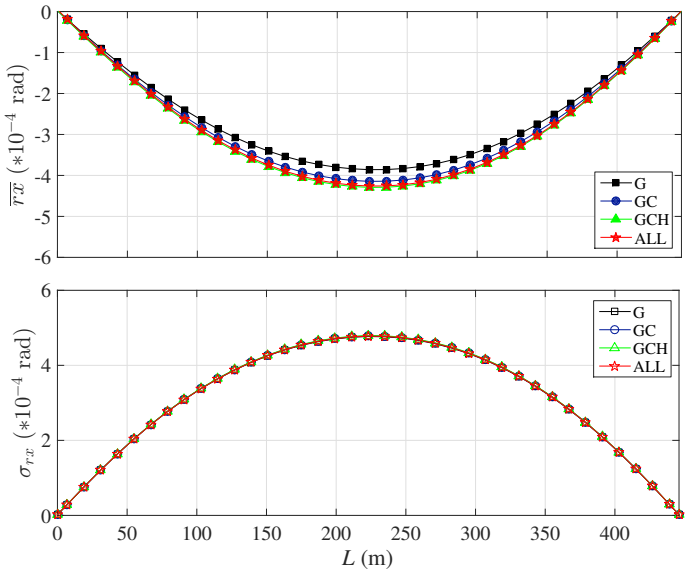

FIGURE 14. Wind induced torsional displacement of the bridge girder considering wind loads on the cable, hanger and tower (top: mean torsional displacement; bottom: torsional displacement standard deviation).

3.3 Time-domain numerical results compared with field measurements

Based on the computed bridge response results presented in the previous section, the time-domain method using the non-linear force model considering the wind loads on the entire bridge is selected to calculate the bridge buffeting response at different mean wind velocities and three different terrain categories. These results are then compared to one-year of field measurement data, as presented in Figs. 15 to 17.

TABLE 7. Discrepancy of the bridge girder response at mid-span when including the wind loads on the girder only (G), the girder + main cables (GC), the girder + hangers + towers (GCH), compared to the case where the wind load is included on the full bridge structure.

	$\bar{y}$	$\bar{z}$	$\overline{rx}$	σ_y	σ_z	σ_{rx}
GCH (%)	-1.2	<0.1	0.8	-0.4	<0.1	0.3
GC (%)	-4.6	-0.2	-2.7	-2.4	<0.1	0.1
G (%)	-10.9	-0.5	-9.4	-6.2	-0.3	-0.2

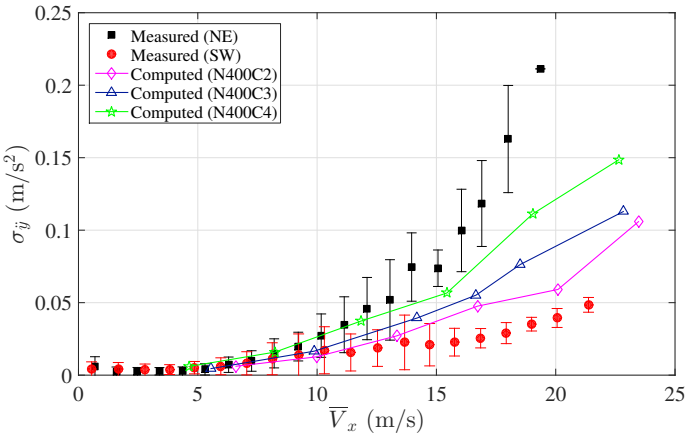

FIGURE 15. Lateral acceleration of the bridge girder, numerical results and full-scale measurements.

The field measurement data corresponds to 10 min acceleration samples recorded continuously from 2015-01-01 to 2015-12-31, among which 10287 samples are associated with the wind from South-West (SW) direction and 5627 samples for the wind from North-East (NE) direction. The field measurement data presented in this section corresponds to the samples characterized by a negligible influence of traffic-induced vibrations on the overall bridge response. Once the separation between NE and SW wind direction is done, the standard deviation of the acceleration is bin averaged into 20 sections, and presented as a function of mean wind velocity normal to the bridge deck $\overline{V}_x$, i.e. considering there is a yaw angle in the field measurements. The variability of the dynamic bridge response at each velocity bin is indicated by the standard deviation of the bridge response inside each bin section. The length of the bar marking the data range is twice the standard deviation of the acceleration response inside each bin section.

In Fig. 15, the monitored lateral response for wind from NE agrees best with the response simulated assuming terrain category 4 (N400C4), while the numerical results using terrain category

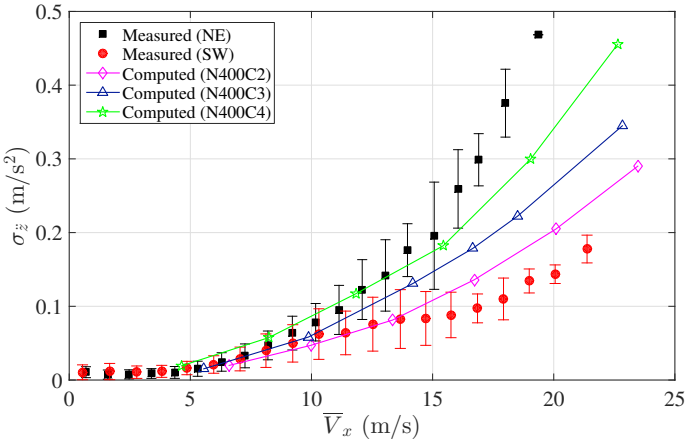

FIGURE 16. Vertical acceleration of the bridge girder, numerical results and full-scale measurements.

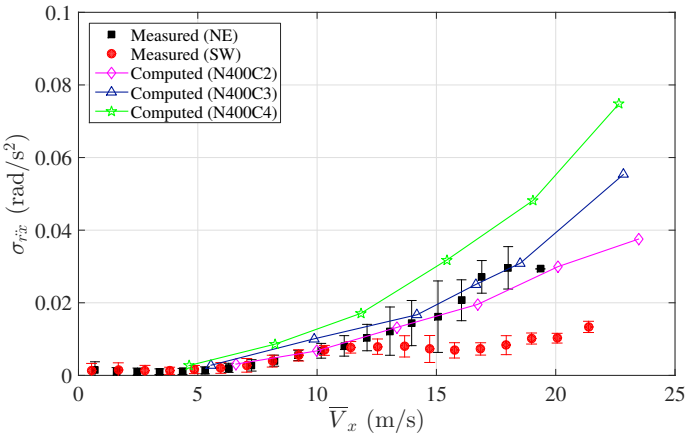

FIGURE 17. Torsional acceleration of the bridge girder, numerical results and full-scale measurements.

2 (N400C2) are closest to the field response data from the SW wind direction. The agreement is especially good for the mean wind velocity lower than 15m/s. It should be noted that for the wind field measurements from the NE direction, the turbulence intensity is quite high, up to 30%. Even with terrain category 4, the turbulence intensity is still not high enough. This may partly explain the discrepancy between the measured and computed responses at high wind velocity.

As the mean wind velocity increases, the full-scale response data deviates significantly, depending on the wind direction, while the numerical results fall in between the field measurements. The difference in the monitored response for the two wind directions is believed to be due to the influence of the terrain on the local wind characteristics. The increasing discrepancy between computed and measured buffeting responses suggests that a customized wind turbulence model should be proposed for such complex terrain topography that involves narrow fjords, mountains and an island. Most importantly, it indicates that the terrain category should be carefully chosen for the design of future fjord-crossing bridges, where wind direction will also be an important factor in determining the correct terrain category, as seen in the Lysefjord Bridge case study. Local wind field observations are therefore essential.

In Fig. 16, a similar trend is observed for the vertical response, where the numerical results replicate well the field measurements at low wind velocities. Again, the numerical results using terrain category 4 (N400C4) agree well with the field measurements from the NE wind direction, and the comparison between the numerical results using terrain category 2 (N400C2) with the field measurements from the SW wind direction is also satisfactory.

Fig. 17 shows that the numerical results slightly overestimated the torsional response, especially for terrain category 4. This is partly because the local wind characteristics may be different from that described in the N400 handbook. We believe that the main reason for the discrepancy seen in the torsional response is that we have at present not included any cross-sectional aerodynamic admittance function, which is likely necessary as the eigen-frequencies for the TS1 and TA1 modes are rather high. This will be refined in the further work.

CONCLUSION

The present study presents the time-domain analysis of the buffeting response of a suspension bridge. The in-service Lysefjord Bridge is used as a study case, which allows a unique comparison of the computational results with full scale response data sampled over a one year period. The time-domain analysis is performed with a finite element model. Turbulent wind field is simulated according to the governing bridge design standard in Norway for three different terrain categories.

The time-domain analysis indicates that the non-linear components of the wind loading are of limited importance in the present case, contributing to the standard deviation of the lateral displacement by less than 5%. The contribution of the buffeting loads on the main cables, hangers and towers to the lateral dynamic response of the bridge girder is about 6%. With the time-domain method, mode coupling, as well as the influences of cables and towers on the bridge response are well captured in the simulation results.

The buffeting response, estimated in terms of the standard deviation of acceleration, are found in good agreement with the one-year field measurement data. The numerical results for terrain category 4 (N400C4) agree quite well with the field measurements from the NE wind direction. Good agreement is seen between the numerical results for terrain category 2 (N400C2) and the field measurements from the SW wind direction. The comparison indicates that the developed numerical method with the non-linear

force model represents the bridge response reasonably well. Further works will aim at an improved statistical significance of the simulations, by increasing the number of simulations per analysis "point", introduction of a cross-sectional admittance function as well as refined modelling of the motion-dependent forces.

The work presented in this paper is a preliminary study, aimed at being useful for further studies of future super-long span bridges proposed for several challenging fjord crossings in Norway. The time-domain non-linear wind buffeting force model and the associated user-defined subroutine scheme within Abaqus, enable us to expand the analysis to suspension bridge designs with the towers on floating foundations, including the hydrodynamic loads on the bridge floating tower. A longer time window is suggested when generating the wind velocity time histories, to achieve a good frequency resolution within the low frequency range of the spectrum, as the planned super-long bridges will have their lowest eigen-frequencies at around 0.01Hz. As a recommendation for the future research, a customized wind turbulence model considering the complicated local topography at the bridge site should be proposed, to provide an improved description of the local wind field. At last, the terrain category should be carefully chosen during the future bridge design.

ACKNOWLEDGMENT

This research was conducted with financial support from the Norwegian Public Roads Administration (NPRA). The assistance by NPRA in performing the full-scale measurements is also gratefully acknowledged.

REFERENCES

[1] Davenport, A. G., 1961. "The application of statistical concepts to the wind loading of structures.". In ICE Proceedings, Vol. 19, pp. 449–472.

[2] Scanlan, R., 1975. "The action of flexible bridges under wind, II: Buffeting theory". *Journal of Sound and Vibration,* ***60***(2), pp. 201 – 211.

[3] Lin, Y., and Yang, J., 1983. "Multimode bridge response to wind excitations". *Journal of Engineering Mechanics,* ***109***(2), pp. 586–603.

[4] Jain, A., Jones, N. P., and Scanlan, R. H., 1996. "Coupled flutter and buffeting analysis of long-span bridges". *Journal of Structural Engineering,* ***122***(7), pp. 716–725.

[5] Xu, Y., and Zhu, L., 2005. "Buffeting response of long-span cable-supported bridges under skew winds. part II: case study". *Journal of Sound and Vibration,* ***281***(35), pp. 675 – 697.

[6] Aas-Jakobsen, K., and Strømmen, E., 2001. "Time domain buffeting response calculations of slender structures". *Journal of Wind Engineering and Industrial Aerodynamics,* ***89***(5), pp. 341 – 364.

[7] Chen, X., Matsumoto, M., and Kareem, A., 2000. "Time domain flutter and buffeting response analysis of bridges". *Journal of Engineering Mechanics*.

[8] Costa, C., Borri, C., Flamand, O., and Grillaud, G., 2007. "Time-domain buffeting simulations for windbridge interaction". *Journal of Wind Engineering and Industrial Aerodynamics,* ***95***(911), pp. 991 – 1006. The Fourth European and African Conference on Wind Engineering.

[9] Petrini, F., Giuliano, F., and Bontempi, F., 2007. "Comparison of time domain techniques for the evaluation of the response and the stability in long span suspension bridges". *Computers & structures,* ***85***(11), pp. 1032–1048.

[10] Cheynet, E., 2016. "Wind-induced vibrations of a suspension bridge: A case study in full-scale". PhD thesis, University of Stavanger, Norway.

[11] Macdonald, J., 2003. Evaluation of buffeting predictions of a cable-stayed bridge from full-scale measurements.

[12] Vegdirektoratet, 2015. *Bruprosjektering Prosjektering av bruer, ferjekaier og andre brende konstruksjoner*. Norwegian public road administration.

[13] Steigen, R. O., 2011. "Modeling and analyzing a suspension bridge in light of deterioration of the main cable wires". Master's thesis, University of Stavanger.

[14] Tveiten, J., 2012. "Dynamic analysis of a suspension bridge". Master's thesis, University of Stavanger.

[15] Dassault Systemes, 2011. Abaqus/standard: User's manual. `http://www.3ds.com/products-services/simulia/products/abaqus/`.

[16] Cheynet, E., Jakobsen, J. B., and Snæbjörnsson, J., 2016. "Buffeting response of a suspension bridge in complex terrain". *Engineering Structures,* ***128***, pp. 474–487.

[17] EN 1991-1-4, 1991. 1-4: 2005 eurocode 1: Actions on structures – general actions – wind actions.

[18] Shinozuka, M., and Jan, C.-M., 1972. "Digital simulation of random processes and its applications". *Journal of sound and vibration,* ***25***(1), pp. 111–128.

[19] Shinozuka, M., and Deodatis, G., 1991. "Simulation of Stochastic Processes by Spectral Representation". *Applied Mechanics Reviews,* ***44***.

[20] Øiseth, O., Rönnquist, A., and Sigbjörnsson, R., 2013. "Effects of co-spectral densities of atmospheric turbulence on the dynamic response of cable-supported bridges: A case study". *Journal of Wind Engineering and Industrial Aerodynamics,* ***116***, pp. 83 – 93.

[21] AAJ, 1999. *Beregninger av egenfrekvenser for lysefjordbrua. Tech.rep.* Statens Vegvesen.